

Article

The “Funny” Current (I_f) Inhibition by Ivabradine at Membrane Potentials Encompassing Spontaneous Depolarization in Pacemaker Cells

Yael Yaniv, Victor A. Maltsev, Bruce D. Ziman, Harold A. Spurgeon and Edward G. Lakatta *

Laboratory of Cardiovascular Science, Intramural Research Program, National Institute on Aging, NIH, 5600 Nathan Shock Dr., Baltimore, MD 21224, USA

* Author to whom correspondence should be addressed; E-Mail: LakattaE@mail.nih.gov; Tel.: +1-410-558-8202; Fax: +1-410-558-8150.

Received: 21 May 2012; in revised form: 3 July 2012 / Accepted: 4 July 2012 /

Published: 9 July 2012

Abstract: Recent clinical trials have shown that ivabradine (IVA), a drug that inhibits the funny current (I_f) in isolated sinoatrial nodal cells (SANC), decreases heart rate and reduces morbidity and mortality in patients with cardiovascular diseases. While IVA inhibits I_f , this effect has been reported at essentially unphysiological voltages, *i.e.*, those more negative than the spontaneous diastolic depolarization (DD) between action potentials (APs). We tested the relative potency of IVA to block I_f over a wide range of membrane potentials, including those that encompass DD governing to the SANC spontaneous firing rate. A clinically relevant IVA concentration of 3 μ M to single, isolated rabbit SANC slowed the spontaneous AP firing rate by 15%. During voltage clamp the maximal I_f was 18 ± 3 pA/pF (at -120 mV) and the maximal I_f reduction by IVA was $60 \pm 8\%$ observed at -92 ± 4 mV. At the maximal diastolic depolarization (~ -60 mV) I_f amplitude was only -2.9 ± 0.4 pA/pF, and was reduced by only $41 \pm 6\%$ by IVA. Thus, I_f amplitude and its inhibition by IVA at physiologically relevant membrane potentials are substantially less than that at unphysiological (hyperpolarized) membrane potentials. This novel finding more accurately describes how IVA affects SANC function and is of direct relevance to numerical modeling of SANC automaticity.

Keywords: pacemaker cell automaticity; pacemaker Ca^{2+} clock; arrhythmia

1. Introduction

Heart rate is a primary determinant of cardiac output, an index of myocardial work and myocardial oxygen demand, an index of ATP production rate. An elevation of resting heart rate, therefore, increases the oxygen demand and when the energy reserve capacity is limited can promote an imbalance between energy demand and supply. Clinical evidence has shown that an increase in heart rate in patients with ischemic heart diseases is associated with an increased cardiovascular morbidity and mortality (e.g., [1,2]), and that drugs which reduce the heart rate can improve myocardial pumping performance and energy balance efficiency. Recent clinical trials (for a review cf. [3]) have shown that administration of ivabradine (IVA), a drug that inhibits I_f , *i.e.*, an inward current activated by hyperpolarization of the cell membrane, is associated with a reduction in heart rate and reduction in morbidity and mortality in patients with cardiovascular diseases.

At concentrations that are achieved by approximately clinical doses, IVA in isolated rabbit SANC *in vitro*, inhibits I_f and has no significant action on other membrane ion channels [4], and has no direct effect on myocardial contractility [5]. The relative reduction in I_f *in vitro* by IVA, however, has been reported only at hyperpolarized membrane potentials, *i.e.*, those more negative to the maximum diastolic potential (MDP), far from the physiological voltages over which I_f can contribute to spontaneous diastolic depolarization (DD) of the surface membrane in rabbit SANC [4,6]. Thus the relative reduction in I_f by IVA over a physiological voltage range is unknown. On the other hand, inhibition of funny-channels by IVA occurs only when they are open [4], *i.e.*, when I_f is activated. Since I_f is activated less at physiological potentials than at hyperpolarized (unphysiological) potentials, we hypothesize that the relative blockade of I_f by IVA is voltage dependent, and may be less at physiologically relevant membrane potentials than at hyperpolarized potentials which have previously been studied. If this were the case, it would indeed be of direct relevance to pacemaker cell normal automaticity as it would allow a more precise portrayal of I_f and its inhibition by IVA in numerical models of the coupled-clock system that regulates normal automaticity.

We found by measuring AP and ionic currents in single isolated SANC, that the IVA blockade is, indeed, less pronounced at physiological membrane potentials, *i.e.*, those encompassing DD (~ -60 mV) than at potentials more negative to the MDP.

2. Results

2.1. IVA Blocks I_f in SANC

Representative examples of I_f as a function of membrane potential during voltage clamp with and without 3 μ M IVA are shown in Figure 1A. The average effect of IVA ($n = 9$ for each IVA concentration) on the I–V relationship of peak I_f is shown in Figure 1B. I_f activation was calculated from the peak tail current 5 min after IVA application (at steady state of blockade). I_f tail density, at each membrane potential is expressed relative to its maximal value at -120 mV in control. The average I_f characteristics in the presence or absence of IVA are summarized in Table 1. On average (Figure 1D) at low concentration (3 μ M), IVA decreased the peak I_f without significantly shifting its activation curve (Table 1), but at higher concentrations of 10 and 30 μ M, IVA shifted the activation curve, *i.e.*, $V_{1/2}$ was shifted to lower potentials from -68 ± 4 to -74 ± 4 and -77 ± 5 mV, respectively.

Figure 1. Effects of IVA on amplitude and activation kinetics over a wide range of membrane potential range. (A) Representative I_f traces in SANC recorded before and after application of IVA and (B) average peak I_f amplitude-voltage relationship; (C) representative I_f tail traces recorded in SANC before and after application of IVA and (D) I_f steady-state activation curve under control conditions and in the presence of different concentrations of IVA (n = 9 for each concentration).

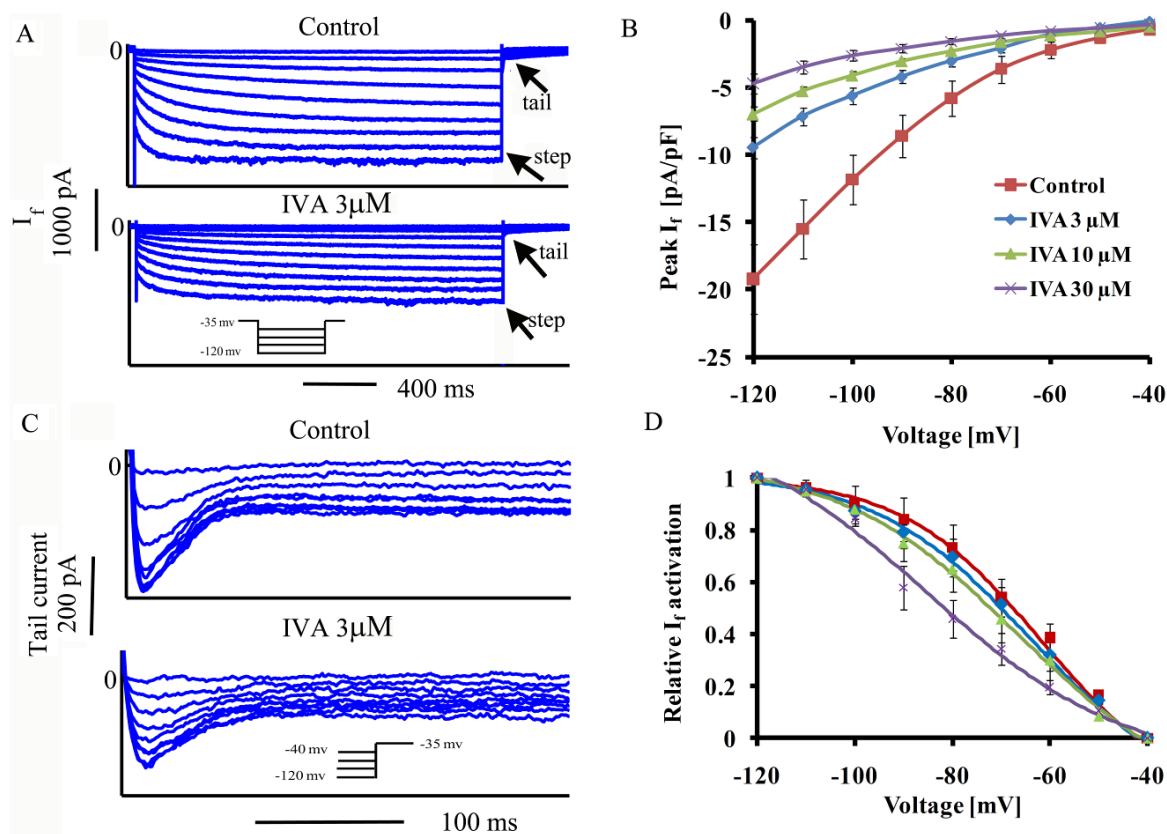


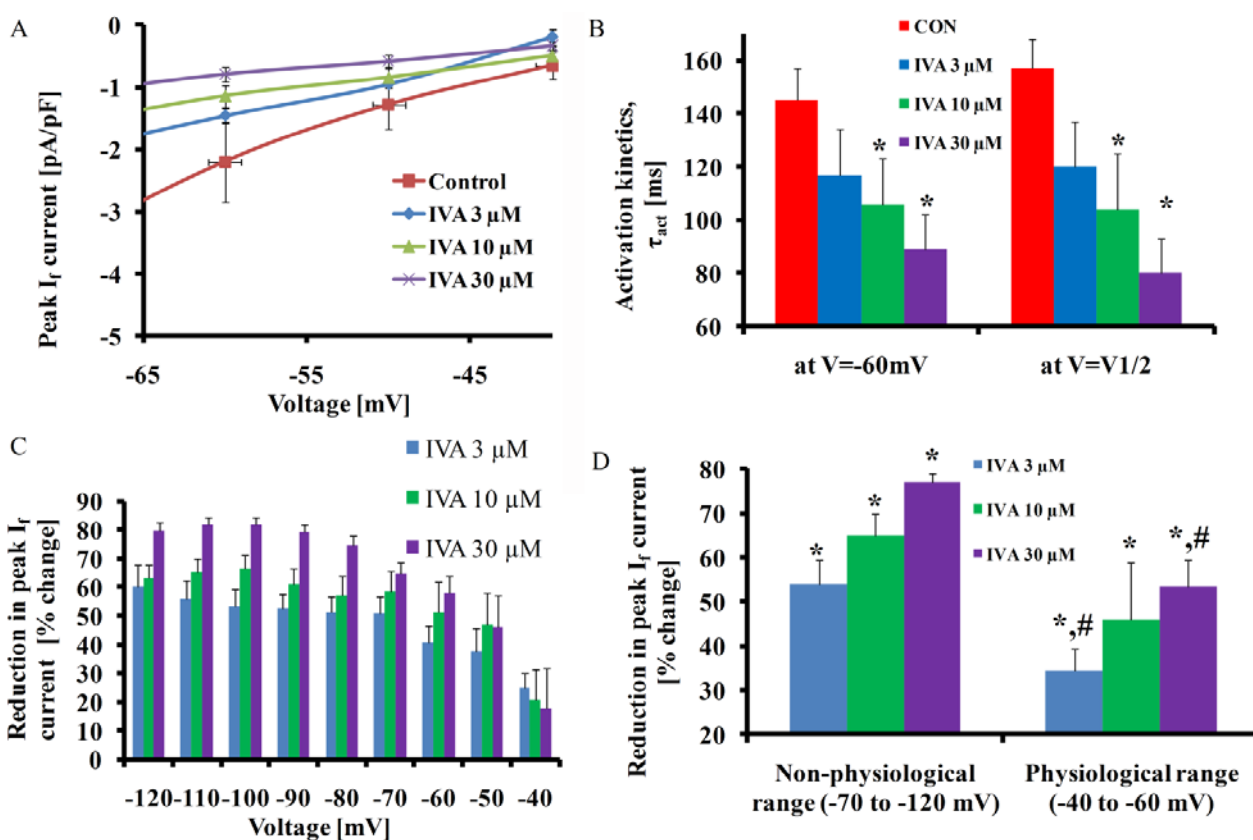
Table 1. I_f characteristics, * $p < 0.05$ vs. control, # $p < 0.05$ vs. ivabradine 3 μM .

	Control	Ivabradine 3 μM (n = 9)	Ivabradine 10 μM (n = 9)	Ivabradine 30 μM (n = 9)
$V_{1/2}$ activation (mV)	-68 ± 4	-70 ± 4 ($p = 0.07$)	-74 ± 4 * ($p = 0.02$)	-77 ± 5 * ($p = 0.04$)
Max τ_{act} (ms)	157 ± 11	120 ± 17 ($P = 0.5$)	106 ± 17 * ($P = 0.05$)	80 ± 13 * ($P = 0.02$)
I_f density (pA/pF) (V = control $V_{1/2}$ activation)	4.5 ± 0.7	2.1 ± 0.3 * ($P = 0.04$)	1.6 ± 0.2 * ($P = 0.008$)	1.1 ± 0.2 *# (0.004)
I_f (pA/pF) (V = MDP)	3 ± 0.43	2 ± 0.3 * ($P = 0.045$)	1.5 ± 0.2 * ($P = 0.04$)	1.3 ± 0.2 * ($P = 0.01$)

On average, at $V_{1/2}$, IVA at 3, 10 and 30 μM IVA (n = 9 for each concentration) decreased the peak I_f by 49 ± 6 , 68 ± 4 , 77 ± 10 percent control, respectively. While the concept of $V_{1/2}$ is instructive in biophysical terms, $I_f V_{1/2}$ occurs at an unphysiological membrane potential, *i.e.*, outside the range over

which the membrane potential in rabbit SANC spontaneously cycles (from -65 to $+30$ mV) during spontaneous AP firing at a rate of ~ 2.5 Hz. Figure 2A illustrates peak I_f as a function of membrane potential over the entire range of DD where I_f has physiological importance by contributing to pacemaker function. Note that I_f amplitude, even in control is small over this voltage range. Figure 2B shows that activation kinetics, expressed as τ_{act} , at -60 mV and $V_{1/2}$, are smaller at larger IVA concentrations. Figure 2C shows the voltage dependence of the reduction in peak I_f by IVA. Note that peak I_f and relative IVA inhibition are higher at unphysiological membrane potentials: on average ($n = 9$ for each IVA concentration) steady-state blockade (95% interval) was achieved at -92 ± 4 , -89 ± 5 and -88 ± 5 mV with 3, 10 and 30 μM IVA, respectively. At the physiological range of membrane potentials (-60 to -40 mV) average reductions in peak I_f were only 34.5 ± 13 , 46 ± 13 and $53.5 \pm 6\%$ with 3, 10 and 30 μM IVA in contrast to 54 ± 5.5 , 65 ± 5 and $77 \pm 2\%$ over the unphysiologic membrane potential range with 3, 10 and 30 μM IVA, respectively (Figure 2D).

Figure 2. Effects of IVA on I_f amplitude and activation kinetics in the physiological membrane potential range. (A) Average peak I_f amplitude-voltage relationship in physiologically range of membrane potential; (B) I_f activation kinetics at physiologic and non-physiologic membrane potentials; (C–D) reduction in I_f amplitude over wide range of membrane potentials including physiological and non-physiological values ($n = 9$ for each concentration). * $p < 0.05$ vs. control, # $p < 0.05$ vs. non-physiological range.



2.2. Concentration-Dependent Block of $I_{Ca,L}$ by IVA in SANC

Concentrations of IVA higher than 3 μM are known also to affect $I_{Ca,L}$ [4]. We measured the effect of IVA on $I_{Ca,L}$ at the concentrations of IVA used to measure the IVA effects on I_f . Representative examples of $I_{Ca,L}$ at a maximal peak current measured at -5 mV and average data of $I_{Ca,L}$ density as a function of membrane potential are presented in Figure 3A–D, respectively. Average $I_{Ca,L}$ characteristics are summarized in Table 2. In the presence of 3 μM IVA, peak $I_{Ca,L}$ decreased by 3.4 ± 1 percent from control (from -13.9 ± 1 to -13.3 ± 1 pA/pF, $n = 12$). This reduction, however, did not statistically differ from $I_{Ca,L}$ run-down ($4.7 \pm 1.5\%$, $n = 9$) in the absence of drug over the 5 min experimental period. At higher concentrations (10 and 30 μM), IVA decreased peak $I_{Ca,L}$ by $22.4 \pm 3\%$ (to -9.9 ± 1.4 pA/pF, $n = 9$) and by $36 \pm 3\%$ (to -8.1 ± 1 pA/pF, $n = 9$), respectively. Figure 3E shows the reduction in $I_{Ca,L}$ as function of the membrane potential. The relative IVA blockade of $I_{Ca,L}$ was maximal at maximal $I_{Ca,L}$ ($V = -5$ mV).

Figure 3. Effect of IVA on $I_{Ca,L}$. (A–C) Representative effect of IVA on maximal $I_{Ca,L}$; (D) average $I_{Ca,L}$ amplitude-voltage relationship under control conditions and in the presence of different IVA concentrations, and (E) relative reduction in $I_{Ca,L}$ as a function of membrane potential ($n = 12$ for control and 3 μM IVA; $n = 9$ for 10 and 30 μM IVA).

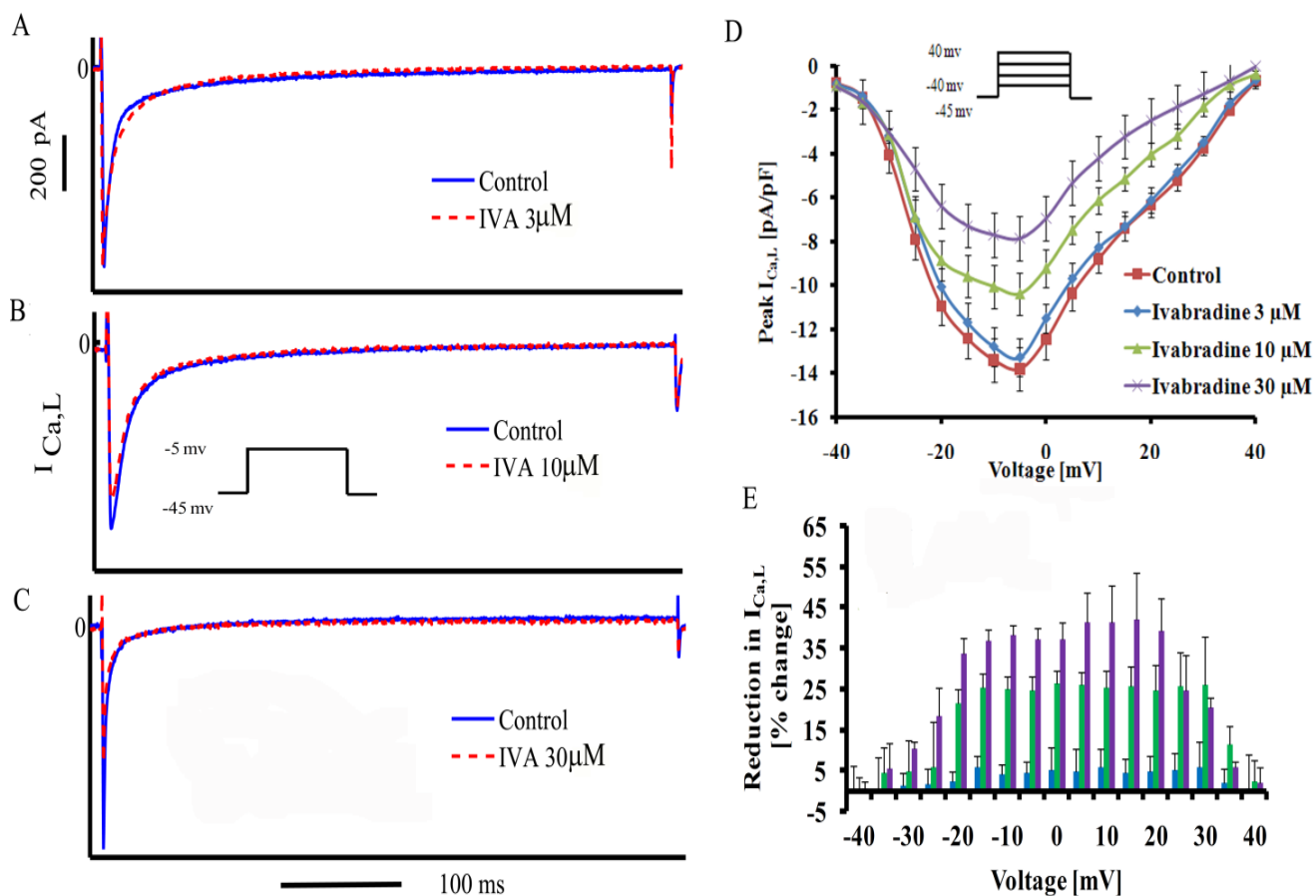


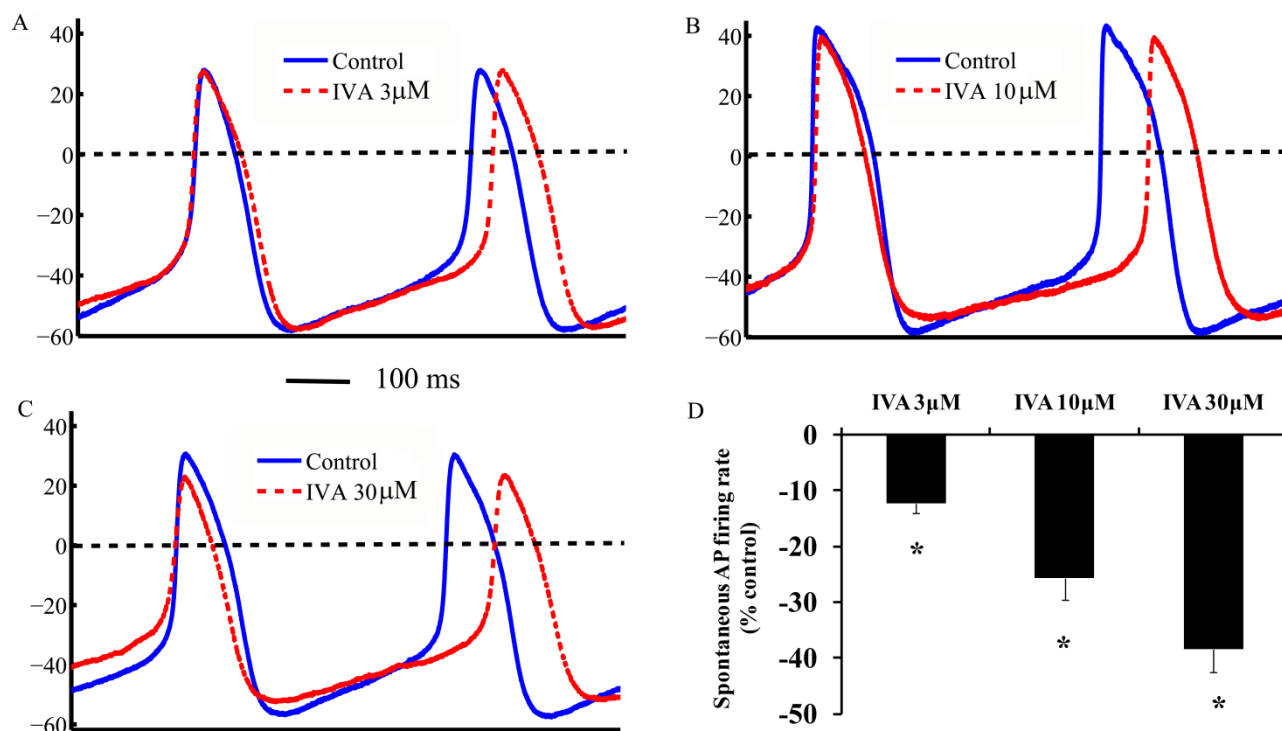
Table 2. $I_{Ca,L}$ characteristics, * $p < 0.05$ vs. control, # $p < 0.05$ vs. IVA 3 μ M.

	Control	Ivabradine 3 μ M (n = 12)	Ivabradine 10 μ M (n = 9)	Ivabradine 30 μ M (n = 9)
Peak $I_{Ca,L}$ density (pA/pF)	13.9 \pm 1	13.2 \pm 1 ($p = 0.953$)	9.85 \pm 1.4 * ($p = 0.0003$)	8.1 \pm 1 *.# ($p < 0.001$)
Voltage at peak $I_{Ca,L}$ (mV)	-5.55 \pm 1	-5.4 \pm 0.7 ($p = 0.84$)	-5 \pm 0.1 ($p = 1$)	-6 \pm 0.8 ($p = 0.98$)

2.3. IVA Reduces the SANC Spontaneous AP Firing Rate

To determine IVA effect on AP firing rate, we superfused IVA onto single SANC generating spontaneous APs. Representative examples of APs and average AP firing rate are presented in Figure 4A–C and average results for AP-induced contraction rate are presented in Figure 4D. The AP-firing rate on average (n = 10 for each concentration) was reduced by 13 \pm 2% (from 175 \pm 2 to 155 \pm 9 beats/min), 26 \pm 4% (to 133 \pm 12 beats/min) and 39 \pm 4% (to 110 \pm 11 beats/min) by 3, 10 and 30 μ M IVA, respectively. Note, in control experiments the time-dependent decrease in beating rate was 3 \pm 1.5%.

Figure 4. Effect of IVA on spontaneous AP firing rate. (A–C) Representative AP recordings and (D) average changes in the rate of AP-induced contractions in the presence of IVA (n = 10 for each concentration). * $p < 0.05$ vs. drug control.

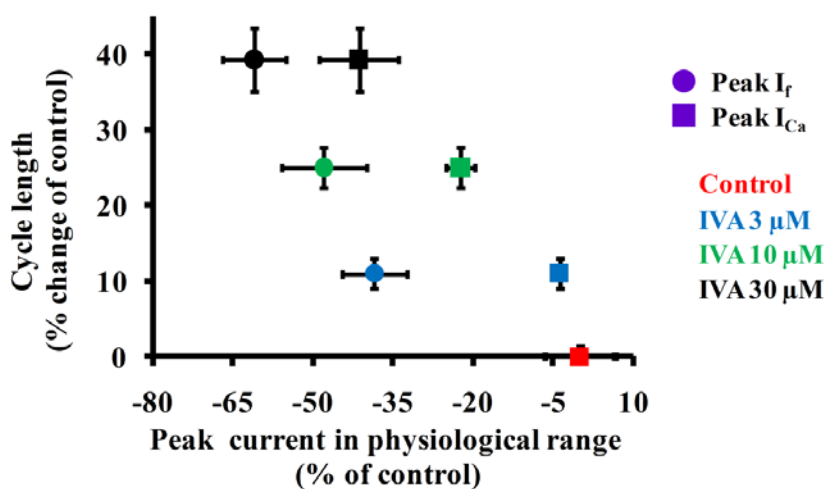


2.4. Correlations Among I_f , $I_{Ca,L}$ and Spontaneous AP Cycle Length in the Absence and Presence of IVA

Figure 5 compares effects of IVA at three concentrations on cycle length as a function of relative reductions of maximal $I_{Ca,L}$ peak or I_f peak over the physiological range of membrane potentials.

A similar concentration dependent block of I_f by IVA (the IVA concentrations vary from 0.1 to 100 μM) and AP firing rate has been reported previously [4]. At low concentration of IVA (3 μM), $I_{Ca,L}$ insignificantly changed, therefore $I_{Ca,L}$ cannot explain the change in spontaneous AP cycle length at this concentration. However, at the two higher concentrations of IVA, $I_{Ca,L}$ is substantially reduced, as also shown previously [4], and at these high IVA concentrations the prolongation in spontaneous AP cycle length is related to reductions in both I_f and $I_{Ca,L}$.

Figure 5. Relationships of AP firing rate as a function of I_f , $I_{Ca,L}$ and AP firing rate. Effect of IVA on the relationship between spontaneous AP cycle length and peak I_f and $I_{Ca,L}$ in physiological range of membrane potentials.



3. Discussion

Because the physiological function of I_f is linked to its contribution to the diastolic depolarization, it is important to characterize the maximal I_f and its activation kinetics within the physiologically relevant range, *i.e.*, above the MDP (~ -60 mV in rabbit SANC). A novel finding of our study is that in SANC, the heart pacemaker cells, the relative IVA blockade of I_f is voltage dependent. At voltages more negative than the MDP, both the I_f amplitude and the I_f blockade by IVA markedly exceed those encountered over the physiological range.

A comprehensive review of the literature on reported I_f amplitude at the MDP compared to its maximal value (-120 mV) is presented in Table 3. Note that on average, I_f amplitude at the MDP (~ -60 mV) is only $\sim 20\%$ of the maximum I_f (~ 14 pA/pF) at -120 mV. Therefore current amplitude and effect of pharmacological interventions and specifically those of I_f and IVA effect should be compared to the pre drug at normal membrane voltages which occur during AP firing, rather than those values measured at more negative, non-physiological voltages. In short, this approach is required to accurately interpret the results of biophysical measurements and pharmacological effects in physiologically relevant terms at physiological potentials and is also critical in the context of numerical modeling of pacemaker function.

Table 3. Biophysical properties of SAN I_f in various species. MDP = Maximum diastolic potential. Values are estimated based on experimental data (from figures) in each of the listed papers.

Species	MDP [mV]	Amplitude at MDP [pA/pF]	Maximal Current at -120 mV [pA/pF]	Reference
Rabbit	-60	8	16	[7]
		10	30	[8]
		1	10	[9]
		1	5	[10]
		1	6	[11]
		1	18	[12]
		1	22	[13]
		4	20	[14]
		4	16	[15]
		3	19	[16]
Mouse	-62	1	6	[17]
		2	11	[18]
		2	22	[19]
		2	15	[20]
		1	20	[21]
Dog	-58	2	15	[22]
		1	6	[18]
		2	10	[23]
Guinea pig	-61	2	11	[24]
		1	12	[25]
Rat	-58	5	15	[26]
Cat	-68	3	6	[27]
Human	-62	1	8	[28]

Because the membrane potential *in vivo* spontaneously cycles within the physiological range, *i.e.*, about from -65 to 30 mV, we explored the reduction in AP firing rate by IVA under physiological conditions by measuring AP-induced contraction, or by utilizing a perforated patch clamp to measure spontaneous AP firing. At $3 \mu\text{M}$, IVA reduced the spontaneous AP firing rate by $13 \pm 2\%$ control (Figure 2), similar to the reduction reported previously in rabbit SANC ($16.2 \pm 1.5\%$ control) [29]. Not in order. Of note, in healthy human volunteers, a bolus of IVA reduces the heart rate during exercise by 10 – 15% , and this effect is sustained for 1 to 12 h [30]. Because IVA inhibition occurs on the inner cell membrane, and only when the I_f channel is open [4], some prior studies have explored the effect of IVA on AP firing rate in SANC following an activation/deactivation protocol via a whole cell voltage clamp [6]. In this protocol, the membrane potential is set as low as to -100 mV every 6 s from a holding potential of -35 mV and then the recording configuration is switched to AP firing in current clamp. A greater reduction in AP firing rate by $3 \mu\text{M}$ IVA ($\sim 25\%$) has been observed in this non-physiological experimental protocol than in the present study [6].

At a clinically relevant concentration, IVA does not alter other cardiovascular functions (*i.e.*, blood pressure, cardiac electrophysiology, *etc.*) [31,32], and therefore it has a potential for therapeutic application by slowing the heart rate. We observed that at low concentrations ($<3 \mu\text{M}$) while IVA

inhibits I_f it does not affect $I_{Ca,L}$ in single isolated rabbit SANC (Figure 2). Similarly, Bois *et al.* [4] showed that low concentrations ($<3 \mu\text{M}$) IVA did not affect $I_{Ca,L}$ current (or I_K current). Note that due to $I_{Ca,L}$ current run-down we cannot distinguish a drug effect that reduces $I_{Ca,L}$ less than 5%. However, our recent SANC coupled-clock numerical model [33] predicts that such a small decrease of 5% in $I_{Ca,L}$ without altering I_f would reduce the spontaneous AP firing rate only by 2% (not shown). At higher IVA concentrations which inhibit $I_{Ca,L}$, $I_{Ca,L}$ inhibition does not directly impact I_f (because I_f is inactivated at voltages lower than -40 mV); the decrease in $I_{Ca,L}$ however, reduces Ca^{2+} influx, and this has a substantial effect to reduce the AP firing rate by directly impacting the Ca^{2+} clock, and by indirectly reducing cAMP production. In this way $I_{Ca,L}$ inhibition by IVA indirectly impacts on I_f current. L-type Ca^{2+} channel is constituted by a pore-forming α_1 subunit. Four L-type α_1 -subunit have been cloned and classified in the Ca_v1 gene family (for review cf. [34]). Recombinant and native $\text{Ca}_v1.3$ -mediated $I_{Ca,L}$ displays a more negative activation and displays a more negative activation threshold than $\text{Ca}_v1.2$. Of note, however, the lower activation threshold for $\text{Ca}_v1.3$ vs. $\text{Ca}_v1.2$ is still more positive to the voltage range where I_f current becomes dominant in mice SANC [35]. Specifically, there is no documentation for a role for $\text{Ca}_v1.3$ in mammalian pacemaker cells other than mice.

Aside from the effect of IVA to reduce the spontaneous AP firing rate of isolated SANC, additional perspectives regarding the role of I_f in spontaneous AP firing rate of SANC require consideration. I_f cannot be the sole mediator of diastolic depolarization, even under normal conditions, because (1) at MDP 54% reduction in I_f (by $30 \mu\text{M}$ IVA, at MDP) mediates an apparent $\sim 40\%$ reduction in spontaneous AP firing rate and not a complete cessation of the heart rate; (2) The relative amplitude of I_f during the diastolic depolarization is much smaller than I_{NCX} , which has also been implicated as a major contributor to diastolic depolarization rate [18,36,37]. Because I_f is larger in SANC from the periphery of the central SAN area than from its center where the AP impulse normally originated [9], and since the peripheral SANC have a lower MDP, the relative effect of IVA on I_f may be stronger in SANC from the peripheral area. In this case, IVA effect would mostly affect the transition of AP to the atria, rather than having a major direct impact on the AP firing.

Although it is impossible to know the exact IVA concentration (diffusion, drug accumulation and *etc.*) achieved at the cellular level in patients, it has been estimated that the concentration is not higher than $3 \mu\text{M}$ [30]. During long treatment protocols in humans, IVA was reported to reduce mean resting heart rate by 11 to 22%, depending on the pre-drug heart rate [30,38]: The IVA-induced decrease in heart rate is higher at higher baseline heart rates. Note, however, that IVA is usually administered to patients in conjunction with a beta-blocker, which also can affect the heart rate [39]. The relative role of I_f may differ among species (Table 3), and this can bias the observed IVA effect on heart rate.

Recent observations in pacemaker cells provide strong evidence that normal automaticity in SANC is regulated by a coupled-clock system: a high basal (*i.e.*, in the absence of β -adrenergic receptor stimulation) Ca^{2+} -activated adenylyl cyclase (AC) drives cAMP/protein kinase-A (PKA), and CaMKII-dependent protein phosphorylations of both surface membrane electrogenic proteins (“membrane clock”), and of sarcoplasmic reticulum (SR) proteins that generate rhythmic Ca^{2+} oscillations (“ Ca^{2+} clock”) [18,36,37]. The degree of protein phosphorylation of the membrane and Ca^{2+} clocks regulates the coupling of the two-clocks, and the periodicity of the coupled clock controls the action potential (AP) rate, *i.e.*, generating the normal automaticity of SANC. Thus the bradycardic effect of IVA may not be interpreted to result solely from its effect to block I_f , a membrane clock

protein because the mutual membrane and Ca^{2+} clock environment and regulation strongly couple the function of both clocks. Changes in AP firing rate generated by a drug effect on the membrane-clock, in a feed-forward manner, will change intracellular Ca^{2+} , and lead to further changes in the AP firing rate. Therefore, the net effect of IVA, even at the low concentration of 3 μM , on AP firing rate of the coupled-clock system may indeed be mediated by effects on both clocks: a direct effect on I_f (a component of the “membrane-clock”) to regulate the AP firing rate, and an indirect effect on the Ca^{2+} clock (due to concomitant reduction in intracellular Ca^{2+} cycling due to clock coupling when the AP firing rate slows). Additional experiments are required to test this interesting possibility.

4. Experimental

4.1. Cell Preparation

Spontaneously beating sinoatrial node cells were isolated from New Zealand White rabbit hearts as previously described [40]. All animal experiments were approved by the Animal Care and Use Committee of the National Institutes of Health (protocol #034LCS2013). The dissociated cells were stored at 4 °C and were used within 10 h of isolation.

4.2. Electrophysiology and Cell Contraction

Spontaneous rhythmic cell contractions during spontaneous AP firing and APs were recorded to quantify the spontaneous AP firing rate in Tyrode solution at 35 ± 0.5 °C, contained the following (in mM): 140 NaCl, 5.4 KCl, 2 MgCl_2 , 5 HEPES, 1.8 CaCl_2 , and 5.5 glucose, and titrated to pH 7.4 with NaOH. The cell suspension was placed in a chamber on an inverted microscope and was allowed to settle for 20 min. Spontaneous cell contractions were measured as previously described [41]. Briefly, cells were imaged with an LSM-510 inverted confocal microscope using a 63x/1.4 N.A. oil immersion lens (Carl Zeiss, Oberkochen, Germany). Transmitted optics linescan images (using 633 nm He-Ne laser excitation, 512x1 pixels at 21.5 pixel/ μm and 0.8 ms/line), were recorded with a scan line oriented along the short axis of the SANC. Spontaneous APs were recorded via a perforated patch-clamp with 35 μM β -escin (Sigma-Aldrich, St. Louis, MO, USA) added to the pipette solution that contained (in mM) the following: 120 K-gluconate, 2.5 NaCl, 2.5 MgATP, 2.5 Na_2ATP , 5 HEPES and 20 KCl, and titrated to pH 7.2 with KOH. SANC contraction and AP measurements were recorded for 5 min under control conditions and 10 min following IVA application.

4.3. I_f Measurements

I_f was measured in whole cell patch clamp mode. Patch pipettes had a resistance of 2–4 M Ω and were filled with solution that contained the following (in mM): 100 K-gluconate, 2.5 MgATP, 2.5 Na_2ATP , 5 HEPES, 20 KCl, 5 EGTA and 2 CaCl_2 and titrated to pH 7.2 with KOH. Tyrode solution (as above) was used as extracellular solution. Membrane series resistance and whole cell and pipette capacities were routinely compensated electronically up to 90%. Voltage steps were applied for 2 s ranging from -120 to -40 mV in 10-mV increments from a holding potential of -35 mV. The voltage steps protocol was applied 3 min after the rupture patch and was repeated every minute for 5 min, following IVA application. The time course of I_f activation (τ) was evaluated by fitting a

monoexponential equation with the Clampfit program (Molecular devices): $I = A (1 - \exp(-t/\tau))$ ignoring the variable initial delay in the current activation [42]. The steady state I_f activation curve was obtained by plotting normalized maximal I_f tail currents at each test potential. The voltage for current half activation ($V_{1/2}$) and the slope factor (s) were characterized by fitting the activation data to Boltzmann equation [42] using the Clampfit program: $I = A/(1 + \exp((V_{1/2}-V)/s))$. The steady state blockade of I_f was defined as 95% of the maximal value. The steady state blockade voltage was calculated by fitting monoexponential equation with the Clampfit program.

4.4. $I_{Ca,L}$ Measurements

$I_{Ca,L}$ was measured in whole cell patch clamp mode. Patch pipettes had a resistance of 2–4 M Ω and were filled with solution that contained (in mM) the following: 110 CsCl, 2.5 MgATP, 2.5 Na₂ATP, 10 HEPES, 5 NaCl, 5 EGTA, 2 CaCl₂ and 20 TEA-Cl, and titrated to pH 7.2 with CsOH. The extracellular solution was the Tyrode solution as described above. Ten μ M tetrodotoxin was added to the Tyrode solution, in the event that interfering currents appeared. Membrane series resistance and whole cell and pipette capacities were routinely compensated electronically up to 90%. Voltage steps ranging from –40 to 40 mV were applied for 300 ms in 5-mV increments from a holding potential of –45 mV (to eliminate interference from $I_{Ca,T}$). The voltage step protocol was applied 3 min after the rupture patch. After IVA application a single step from –45 to 0 mV was applied for 300 ms every 15 s. The voltage steps protocol was applied again 5 min following IVA application. The reductions in I_{Ca} in the range of higher concentrations of IVA are comparable with the results of Bois *et al.* [4], who measured this current in the presence of GTP in the patch pipette. For both cell contraction and electrophysiological recordings, cells from at least five rabbits were used.

4.5. Drugs

IVA was obtained from TRC (Toronto, ON, Canada). All other chemicals were purchased from Sigma-Aldrich.

4.6. Statistical Analysis

Data are presented as mean \pm SEM. For multiple pharmacologic applications, a linear mixed-effects model was used with Dunnett's method to adjust p -values. This model accounts for repeated measurements on the same preparation while allowing testing for differences among different IVA concentrations. $p < 0.05$ was taken to indicate statistical significance.

5. Conclusions

In summary, measuring the relative role of I_f under physiological membrane voltages is required to interpret the results of biophysical measurements and pharmacological effects in physiologically relevant terms and in the context of numerical pacemaker models. The present study shows that the relative IVA blockade of I_f is voltage dependent: at 37 °C in rabbit SANC and at membrane potentials negative to the MDP (unphysiological voltages) both the I_f current amplitude and the effect of IVA to block I_f are higher than at membrane potentials incurred during diastolic depolarization (–65 to –55 mV).

Acknowledgment

The work was supported entirely by the Intramural Research Program of the National Institute on Aging, National Institutes of Health.

Conflicts of Interest

The authors declare no conflict of interest.

References

1. Mensink, G.B.; Hoffmeister, H. The relationship between resting heart rate and all-cause, cardiovascular and cancer mortality. *Eur. Heart J.* **1997**, *18*, 1404–1410.
2. Palatini, P. Heart rate as an independent risk factor for cardiovascular disease: Current evidence and basic mechanisms. *Drugs* **2007**, *67* (Suppl. 2), S3–S13.
3. Riccioni, G. Ivabradine: Recent and potential applications in clinical practice. *Expert Opin. Pharmacother.* **2011**, *12*, 443–450.
4. Bois, P.; Bescond, J.; Renaudon, B.; Lenfant, J. Mode of action of bradycardic agent, S 16257, on ionic currents of rabbit sinoatrial node cells. *Br. J. Pharmacol.* **1996**, *118*, 1051–1057.
5. Boldt, A.; Gergs, U.; Ponicke, K.; Simm, A.; Silber, R.E.; Neumann, J. Inotropic effects of ivabradine in the mammalian heart. *Pharmacology* **2010**, *86*, 249–258.
6. Bucchi, A.; Baruscotti, M.; DiFrancesco, D. Current-dependent block of rabbit sino-atrial node I_f channels by ivabradine. *J. Gen. Physiol.* **2002**, *120*, 1–13.
7. Accili, E.A.; Robinson, R.B.; DiFrancesco, D. Properties and modulation of I_f in newborn versus adult cardiac SA node. *Am. J. Physiol.* **1997**, *272*, H1549–H1552.
8. Goethals, M.; Raes, A.; van Bogaert, P.P. Use-dependent block of the pacemaker current I_f in rabbit sinoatrial node cells by zatebradine (UL-FS 49). On the mode of action of sinus node inhibitors. *Circulation* **1993**, *88*, 2389–2401.
9. Honjo, H.; Boyett, M.R.; Kodama, I.; Toyama, J. Correlation between electrical activity and the size of rabbit sino-atrial node cells. *J. Physiol.* **1996**, *496*, 795–808.
10. Lei, M.; Cooper, P.J.; Camelliti, P.; Kohl, P. Role of the 293b-sensitive, slowly activating delayed rectifier potassium current, i_{Ks} , in pacemaker activity of rabbit isolated sino-atrial node cells. *Cardiovasc. Res.* **2002**, *53*, 68–79.
11. Li, J.; Qu, J.; Nathan, R.D. Ionic basis of ryanodine's negative chronotropic effect on pacemaker cells isolated from the sinoatrial node. *Am. J. Physiol.* **1997**, *273*, H2481–H2489.
12. Lyashkov, A.E.; Vinogradova, T.M.; Zahanich, I.; Li, Y.; Younes, A.; Nuss, H.B.; Spurgeon, H.A.; Maltsev, V.A.; Lakatta, E.G. Cholinergic receptor signaling modulates spontaneous firing of sinoatrial nodal cells via integrated effects on PKA-dependent Ca^{2+} cycling and I_{KACH} . *Am. J. Physiol. Heart Circ. Physiol.* **2009**, *297*, H949–H959.
13. Noble, D.; Denyer, J.C.; Brown, H.F.; DiFrancesco, D. Reciprocal role of the inward currents i_b , i_{Na} and i_f in controlling and stabilizing pacemaker frequency of rabbit sino-atrial node cells. *Proc. Biol. Sci.* **1992**, *250*, 199–207.
14. Satoh, H. $[Ca^{2+}]_i$ -dependent actions of taurine in spontaneously beating rabbit sino-atrial nodal cells. *Eur. J. Pharmacol.* **2001**, *424*, 19–25.

15. Verheijck, E.E.; van Ginneken, A.C.; Wilders, R.; Bouman, L.N. Contribution of L-type Ca^{2+} current to electrical activity in sinoatrial nodal myocytes of rabbits. *Am. J. Physiol.* **1999**, *276*, H1064–H1077.
16. Verkerk, A.O.; den Ruijter, H.M.; Bourier, J.; Boukens, B.J.; Brouwer, I.A.; Wilders, R.; Coronel, R. Dietary fish oil reduces pacemaker current and heart rate in rabbit. *Heart Rhythm.* **2009**, *6*, 1485–1492.
17. Verkerk, A.O.; Wilders, R.; Zegers, J.G.; van Borren, M.M.; Ravesloot, J.H.; Verheijck, E.E. Ca^{2+} -activated Cl^- current in rabbit sinoatrial node cells. *J. Physiol.* **2002**, *540*, 105–117.
18. Gao, Z.; Chen, B.; Joiner, M.L.; Wu, Y.; Guan, X.; Koval, O.M.; Chaudhary, A.K.; Cunha, S.R.; Mohler, P.J.; Martins, J.B.; *et al.* I_f and SR Ca^{2+} release both contribute to pacemaker activity in canine sinoatrial node cells. *J. Mol. Cell. Cardiol.* **2010**, *49*, 33–40.
19. Mangoni, M.E.; Nargeot, J. Properties of the hyperpolarization-activated current (I_f) in isolated mouse sino-atrial cells. *Cardiovasc. Res.* **2001**, *52*, 51–64.
20. Rose, R.A.; Kabir, M.G.; Backx, P.H. Altered heart rate and sinoatrial node function in mice lacking the cAMP regulator phosphoinositide 3-kinase-gamma. *Circ. Res.* **2007**, *101*, 1274–1282.
21. Rose, R.A.; Lomax, A.E.; Kondo, C.S.; Anand-Srivastava, M.B.; Giles, W.R. Effects of C-type natriuretic peptide on ionic currents in mouse sinoatrial node: A role for the NPR-C receptor. *Am. J. Physiol. Heart Circ. Physiol.* **2004**, *286*, H1970–H1977.
22. Springer, J.; Azer, J.; Hua, R.; Robbins, C.; Adamczyk, A.; McBoyle, S.; Bissell, M.B.; Rose, R.A. The natriuretic peptides BNP and CNP increase heart rate and electrical conduction by stimulating ionic currents in the sinoatrial node and atrial myocardium following activation of guanylyl cyclase-linked natriuretic peptide receptors. *J. Mol. Cell. Cardiol.* **2012**, *52*, 1122–1134.
23. Protas, L.; Oren, R.V.; Clancy, C.E.; Robinson, R.B. Age-dependent changes in Na current magnitude and TTX-sensitivity in the canine sinoatrial node. *J. Mol. Cell. Cardiol.* **2010**, *48*, 172–180.
24. Yeh, Y.H.; Burstein, B.; Qi, X.Y.; Sakabe, M.; Chartier, D.; Comtois, P.; Wang, Z.; Kuo, C.T.; Nattel, S. Funny current downregulation and sinus node dysfunction associated with atrial tachyarrhythmia: A molecular basis for tachycardia-bradycardia syndrome. *Circulation* **2009**, *119*, 1576–1585.
25. Kojima, A.; Kitagawa, H.; Omatsu-Kanbe, M.; Matsuura, H.; Nosaka, S. Inhibitory effects of sevoflurane on pacemaking activity of sinoatrial node cells in guinea-pig heart. *Br. J. Pharmacol.* **2012**, doi:10.1111/j.1476-5381.2012.01914.x.
26. Satoh, H. Electropharmacology of taurine on the hyperpolarization-activated inward current and the sustained inward current in spontaneously beating rat sino-atrial nodal cells. *J. Pharmacol. Sci.* **2003**, *91*, 229–238.
27. Zhou, Z.; Lipsius, S.L. Properties of the pacemaker current I_f in latent pacemaker cells isolated from cat right atrium. *J. Physiol.* **1992**, *453*, 503–523.
28. Verkerk, A.O.; Wilders, R.; van Borren, M.M.; Peters, R.J.; Broekhuis, E.; Lam, K.; Coronel, R.; de Bakker, J.M.; Tan, H.L. Pacemaker current (I_f) in the human sinoatrial node. *Eur. Heart J.* **2007**, *28*, 2472–2478.
29. Bucchi, A.; Baruscotti, M.; Robinson, R.B.; DiFrancesco, D. Modulation of rate by autonomic agonists in SAN cells involves changes in diastolic depolarization and the pacemaker current. *J. Mol. Cell. Cardiol.* **2007**, *43*, 39–48.

30. Borer, J.S.; Le Heuzey, J.Y. Characterization of the heart rate-lowering action of ivabradine, a selective I(f) current inhibitor. *Am. J. Ther.* **2008**, *15*, 461–473.
31. Camm, A.J.; Lau, C.P. Electrophysiological effects of a single intravenous administration of ivabradine (S 16257) in adult patients with normal baseline electrophysiology. *Drugs R D* **2003**, *4*, 83–89.
32. Simon, L.; Ghaleh, B.; Puybasset, L.; Giudicelli, J.F.; Berdeaux, A. Coronary and hemodynamic effects of S 16257, a new bradycardic agent, in resting and exercising conscious dogs. *J. Pharmacol. Exp. Ther.* **1995**, *275*, 659–666.
33. Maltsev, V.A.; Lakatta, E.G. A novel quantitative explanation for the autonomic modulation of cardiac pacemaker cell automaticity via a dynamic system of sarcolemmal and intracellular proteins. *Am. J. Physiol. Heart Circ. Physiol.* **2010**, *298*, H2010–H2023.
34. Mangoni, M.E.; Nargeot, J. Genesis and regulation of the heart automaticity. *Physiol. Rev.* **2008**, *88*, 919–982.
35. Mangoni, M.E.; Couette, B.; Bourinet, E.; Platzer, J.; Reimer, D.; Striessnig, J.; Nargeot, J. Functional role of L-type Cav1.3 Ca²⁺ channels in cardiac pacemaker activity. *Proc. Natl. Acad. Sci. USA* **2003**, *100*, 5543–5548.
36. Bogdanov, K.Y.; Vinogradova, T.M.; Lakatta, E.G. Sinoatrial nodal cell ryanodine receptor and Na⁺-Ca²⁺ exchanger: molecular partners in pacemaker regulation. *Circ. Res.* **2001**, *88*, 1254–1258.
37. Shinohara, T.; Park, H.W.; Joung, B.; Maruyama, M.; Chua, S.K.; Han, S.; Shen, M.J.; Chen, P.S.; Lin, S.F. Selective sinoatrial node optical mapping and the mechanism of sinus rate acceleration. *Circ. J.* **2012**, *76*, 309–316.
38. Bohm, M.; Swedberg, K.; Komajda, M.; Borer, J.S.; Ford, I.; Dubost-Brama, A.; Lerebours, G.; Tavazzi, L. Heart rate as a risk factor in chronic heart failure (SHIFT): The association between heart rate and outcomes in a randomised placebo-controlled trial. *Lancet* **2010**, *376*, 886–894.
39. Amosova, E.; Andrejev, E.; Zaderey, I.; Rudenko, U.; Ceconi, C.; Ferrari, R. Efficacy of ivabradine in combination with Beta-blocker versus uptitration of Beta-blocker in patients with stable angina. *Cardiovasc. Drugs Ther.* **2011**, *25*, 531–537.
40. Vinogradova, T.M.; Sirenko, S.; Lyashkov, A.E.; Younes, A.; Li, Y.; Zhu, W.; Yang, D.; Ruknudin, A.M.; Spurgeon, H.; Lakatta, E.G. Constitutive phosphodiesterase activity restricts spontaneous beating rate of cardiac pacemaker cells by suppressing local Ca²⁺ releases. *Circ. Res.* **2008**, *102*, 761–769.
41. Yaniv, Y.; Juhaszova, M.; Lyashkov, A.E.; Spurgeon, H.; Sollott, S.J.; Lakatta, E.G. Ca²⁺-regulated-cAMP/PKA signaling in cardiac pacemaker cells links ATP supply to demand. *J. Mol. Cell. Cardiol.* **2011**, *51*, 740–748.
42. van Ginneken, A.C.; Giles, W. Voltage clamp measurements of the hyperpolarization-activated inward current I_f in single cells from rabbit sino-atrial node. *J. Physiol.* **1991**, *434*, 57–83.

Sample Availability: Not available.